FERROXANE DERIVED CERAMIC COMPOSITE MATERIAL AS CATALYSTS FOR HETEROGENOUS FENTON REACTIONS FOR DYES AND PHARMACEUTICAL REMOVAL IN WATER.

A Thesis

Presented to the Faculty of the Graduate School

at the University of Missouri-Columbia

In Partial Fulfillment

of the Requirements for the Degree

Master of Science

By

Mohammed Hussain

Dr. Maria Fidalgo, Thesis Supervisor

DECEMBER 2016

The undersigned, appointed by the Dean of the Graduate School, have examined the thesis entitled:

FERROXANE DERIVED CERAMIC COMPOSITE MATERIAL AS CATALYSTS FOR HETEROGENEOUS FENTON REACTIONS FOR DYES AND PHARMACEUTICAL REMOVAL IN WATER.

Presented by Mohammed Hussain,

A candidate for the degree of Master of Science,

And hereby certify that, in their opinion, it is worthy of acceptance.

_____

Dr. Maria Fidalgo

_____

Dr. Enos C. Inniss

_____

Dr. Chung-ho Lin

ACKNOWLEDGEMENTS

First, I would to express my sincere gratitude to my advisor, Dr. Maria Fidalgo for the continuous support of my study and research, for her patience, motivation, enthusiasm, and immense knowledge. I could not have wished for a better advisor!

I also want to thank Dr. Enos Inniss, my mentor, my friend, for his guidance and support over the years. The undergraduate research opportunity he offered me gave me a strong foundation in research and work experience that eased my master's research.

I would also like to thank Dr. Chung-ho Lin for accepting to be on my committee on a short notice, and for his sincere kindness and support with my research.

To my lab mates, Mohamed Bayati, Abbas Kadhem, Fadi Tantish, and Mohammed Numaan whose support and friendship helped form my work. Special thanks to Atri, Max Storms and Jingjing Dai for their great kindness, support, friendship, and the amount of help they offered with my research.

To my undergraduate students, Shannon Kelly, Danny Shannon, and David Comer for their work, patience, and motivation. Special thanks to Shannon Kelly for the tremendous amount of work she did over a short period of time, and for reviewing my thesis.

Most importantly, to my biggest supporters, my family. To my mom and dad, my brothers, Bilal and Karim, and my sister, Afnan, for the support, the love, the happiness, and the continues guidance. I hope I made you proud!

Finally, to the University of Missouri. For her columns, her people, Rec center, intramurals, and the opportunities she's given me. For the best 6 years of my life!

Mizou-rah!

TABLE OF CONTENTS

LIST OF FIGURES

LIST OF TABLES

ABSTRACT

The goal of this project is to fabricate iron oxide (ferroxane) ceramics as catalysts for heterogeneous Fenton reactions, which will ultimately be used in the degradation of non-biodegradable organic compounds, such as pharmaceuticals, in water. Iron oxide ceramics were fabricated from carboxylate-FeOOH nanoparticles (Ferroxane). Their synthesis took place in two steps: (i) synthesis of γ-FeO(OH) (lepidocrocite) from ferrous chloride; and (ii) ferroxane production from the mineral by reacting it with acetic acid. Hematite was obtained by sintering ferroxane nanoparticles at 500 C^o. Next, ferroxane nanoparticles were reacted with salts of cobalt and manganese, due to their high reduction potential, to obtain mixed metal oxide nanoparticles at 10:1, 4:1, and 2:1 Fe:metal ratio.

Ferroxane-derived ceramics and metal doped ferroxane were characterized by particle size, zeta potential, specific surface area, and chemical composition, which was done by using Dynamic Light Scattering (DLS), Brunauer–Emmett–Teller (BET), powder X-ray diffraction (XRD), and Scanning Electron Microscopy images combined with Energy Dispersive X-ray Spectroscopy (EDS). Size and zeta potential measurements were conducted in the 3-9 pH range in order to assess modifications introduced by the doping reactions and obtain the point of zero charge (pzc). Ferroxane, Co doped ferroxane, and Mn doped ferroxane had pzc at 7.8, 7.3, and 8.2 respectively. Moreover, size remained mostly unchanged by doping when compared to the pure iron oxide particles (200nm - 400nm) for all pHs except the highest, where significant aggregation was observed for some samples. Ferroxane and hematite had surface areas of 72.47 and 23.24 m^2/g respectively. XRD results showed identical peaks to lepidocrocite and hematite, which

confirmed the synthesis process of those metals. EDS results showed peaks of Co and Mn in the doped samples, which proves the success of the doping process.

The catalytic activity of hematite and metal doped ferroxane were tested by adding 8g/l of catalyst, 10 ppm methylene blue (MB), 400 mM H_2O_2, and UV_{365} to a reactor, while measuring the concentration of MB through a spectrophotometer at 665 nm. At pH 7.6, hematite achieved 100% MB degradation during 2 hours of reaction, while Co doped ferroxane achieved 80% and and Mn doped ferroxane achieved 40%. However, the metals doped ferroxane achieved faster degradation compared to hematite during the first 20 minutes. In addition, when the pH was raised to 8.0, Mn doped ferroxane achieved 60% degradation over 2 hours. The following shows potential for greater catalytic activity of the doped ferroxane by optimizing the pH (close to the pzc) and amount of H_2O_2 added. Finally, the catalytic activity of hematite was tested on two antibiotics commonly found in wastewater: sulfamethazine and Oxytetracycline. Solution concentration of 1ppm was used. Hematite achieved 80% degradation of sulfamethazine over two hours, and 100% Oxytetracycline adsorption within 10 minutes.

Future work will involve further characterization of supported particles on surface of ceramic membranes, and optimization of metal doped ferroxane degradation experiments.

1 Introduction

Pharmaceuticals are synthetic or natural chemicals that can be found in prescription medicines or over-the-counter drugs, and drugs used for animals. Pharmaceuticals can enter water sources through sewage, which transports the waste of individuals and patients who have used these chemicals, from uncontrolled drug disposal, such discarding drugs into toilets, and from agricultural runoff. Trace amounts of pharmaceuticals, reportedly measured in parts per billion or trillion, including antibiotics, hormones, and mood stabilizers are in our drinking water supplies. Although levels are low, pharmaceuticals are chemicals of emerging concern to the public because of their potential health effects on humans and animals even at those low doses.

Antibiotics are commonly used for livestock to promote their growth and to prevent and treat diseases. Residues of antibiotics were found in livestock's manure, which is intended to be used as fertilizer on farm fields. Farm products such as corn, potatoes and lettuce can absorb antibiotics when manure is applied. Furthermore, the antibiotics may accumulate, which increases their concentration levels in soil and farm products. This will result in undesirable health effects on humans, animals and ecosystems, since the overuse of antibiotics reduces the ability to cure infections and over time certain antibiotics are rendered ineffective as microorganisms develop resistance through natural selection.

Antibiotics are not treatable by biological processes, and therefore, it's necessary to find another cost effective method to treat those non-biodegradable compounds. The use of advanced oxidation processes (AOPs), such as Fenton processes, for the treatment of non-biodegradable compounds can be an effective way to remove pharmaceuticals from water streams.

In this project, a novel iron oxide (ferroxane) based nanostructured ceramic membranes will be synthesized as catalyst for heterogeneous Fenton, which can be used for the degradation of pharmaceuticals in water. Iron oxides are interesting materials for ceramic membranes due to their efficient catalytic properties, adsorption properties, low cost and limited toxicity. However, there are no commercially available iron oxide membranes to date.

The goal of this project is to fabricate iron oxide (ferroxane) ceramic membranes as catalysts for heterogeneous Fenton reactions, which will ultimately be used in the degradation of non-biodegradable organic compounds, such as pharmaceuticals, in water. This project was developed due the increasing concern about the effect of pharmaceuticals in water, and the need for effective, economical method for treatment.

2 OBJECTIVES

The overall goal of this project is to assess the applicability of a novel iron oxide-based nanostructured catalyst, fabricated through an environmentally friendly route for treatment of antibiotics in wastewater by heterogeneous Fenton reaction. The specific objectives of the project are:

1. To fabricate ferroxane and Mn, Co doped-ferroxane nanoparticles.
2. To characterize the new materials with regard to their particle size, specific surface area, and chemical composition.
3. To synthesize porous hematite particles from ferroxane nanoparticles.
4. To investigate the degradation rates by heterogeneous Fenton process catalyzed by Hematite and Mn, Co doped-ferroxane nanoparticles of methylene blue and two antibiotics, Sulfamethazine and Oxytetracycline, commonly found in wastewater.

3 Literature Review

3.1 Iron Oxide

Iron is one of the most abundant elements on earth, mostly existing in the form of iron oxides. They are used in paints, chemicals sorbents, and catalysts. There are 16 kinds of iron oxides and hydroxides known to date, and these are listed in Table 3.1 below:

Table 3.1- Natural Occurring Iron Oxides [1]

Class	Name	Formula
Iron (II) oxide	Wustite	FeO
Iron(II, III) oxide	Magnetite	Fe_2O_3
Alpha phase Iron (III) oxide		α-Fe_2O_3
beta phase Iron (III) oxide		β- Fe_2O_3
gamma phase Iron (III) oxide	Maghemite	γ- Fe_2O_3
epsilon phase Iron (III) oxide		ε- Fe_2O_3
Iron (II) hydroxide		$Fe(OH)_2$
Iron (III) hydroxide	bernalite	$Fe(OH)_3$
Iron (III) oxide-hydroxide	geothite	α-FeOOH
	akaganetite	β-FeOOH
	lepidocrocite	γ-FeOOH
	feroxyhyte	δ-FeOOH
	ferrihydrite	$FeOOH{\cdot}0.4H_2O$
	schwertmannite	High Pressure FeOOH
	green rusts	$Fe_8O_8(OH)_6(SO)\cdot nH_2O$
		$(Fe^{III}_xFe^{II}_y(OH)_{3x+2y-z}(A^-)_z)$

The iron oxides' structures are octahedron and are composed of Fe and O/OH. There are five polymorphs of FeOOH and four of Fe_2O_3, as seen in Table 3.1. Due to their low solubility, high stability, and high surface area, iron oxides are very effective sorbents for a large range of dissolved ions and molecules[1]. The particle size of most natural iron oxides is less than 200 nm, and most of them can absorb light up to 600 nm, which allows

them to play the role of the photocatalysts in chemical reactions[2-4]. The forms of iron oxides relevant to this research are briefly described below:

- Lepidocrocite (γ-FeOOH) is orange colored and occurs in rocks, soils, biota, and rust, and is often the oxidation product of Fe(II). Its structure is based on the cubic close-packing of anions[4]. The surface area of synthetic Lepidocrocite ranges from 15 to 260 m^2/g[5].

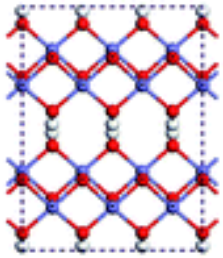

Figure 3.1- Lepidocrocite structure. Red, blue and white dots represent O, Fe and H respectively.

- Hematite (α-Fe_2O_3) is the oldest known iron oxide mineral, and it is most available in rocks and soils. It is red colored and based on a hexagonal close-packing of anions. It is usually the end result of the transformation of iron oxides. The surface area of synthetic hematite ranges from 2 to 200 m^2/g[4].

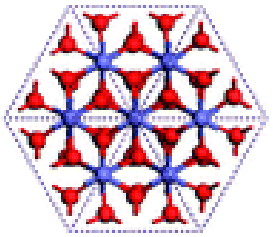

Figure 3.2- Hematite structure. Red, blue and white dots represent O, Fe and H respectively.

- Magnetite (Fe_2O_3) is a black magnetic form of iron oxide, and it is usually responsible for the magnetic properties of rocks. It contains both Fe(II) and Fe(III) and has an inverse spinel structure. The surface area of magnetite ranges from 4 to 100 m^2/g[4, 5].

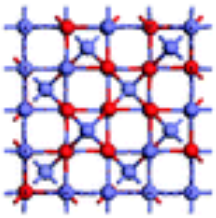

Figure 3.3- Magnetite structure. Red, blue and white dots represent O, Fe and H respectively.

3.2 Methylene blue

About 15% of the total world production of dyes is lost during the dyeing process and released in wastewater[6] . Methylene blue is used in dye, paint production and wool dyeing, microbiology, surgery, diagnostics, and groundwater tracing. The effluent containing dyes are highly colored, resulting in major environmental problems. Methylene blue has good mechanical and chemical stability, and resistant to microbiological degradation due to its complex structure [7]. The chemical structure of methylene blue, $C_{16}H_{18}ClN_3S$, is shown in figure 3.4 below:

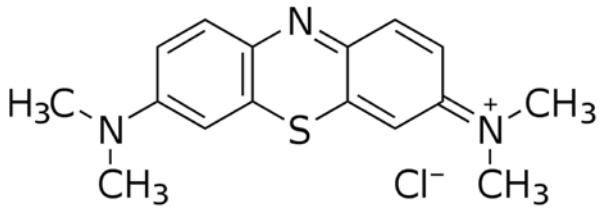

Figure 3.4- Molecular structure of methylene blue dye

Exposure to methylene blue is considered to be toxic as it was found to cause increase in heart rate, vomiting, Heinz body formation, corneal injury, bulbar staining, and urine discoloration[8].

Several methods are used in removing methylene blue: physical methods, mainly adsorption on various supports, such as activated carbon[6]; biological methods, such as biodegradation have been proposed, but due to the low biodegradability of methylene blue, conventional biological waste water treatment processes are not efficient. Chemical treatment processes (ozonation and chlorination) are more effective[7]. In this paper, photocatalytic degradation over solid support for degradation of Methylene blue is proposed.

3.3 Antibiotics: Sulfamethazine and Oxytetracycline

The concern about antibiotic pollution of the environment in water and aquatic ecosystems is increasing globally. Antibiotics are one of the most important medicines and are widely used in animal agriculture to prevent diseases and promote growth [9-11]. Residues of antibiotics have been detected in animals manure, which is usually used as fertilizer for plants growth[12, 13]. When the manure is applied, farm products such as corn, potatoes and lettuce absorb antibiotics [14]. Over time, the antibiotics accumulate, creating increasing concentration levels in the soil and plants [13, 15, 16]. This will result in undesirable health effects on humans, animals, and the ecosystem [17, 18]. The occurrence of antibiotics in the aquatic environment might promote the selection of antibiotic resistance genes and antibiotic resistant bacteria [19]. Antibiotics can also cause asthma and allergies for children[20].

Antibiotics are not degradable by biological processes due to their antibacterial nature [21]. Therefore, chemical approach for degradation of antibiotics is needed. The use of advanced oxidation processes (AOPs), such as Fenton processes for the treatment of non-biodegradable compounds can be an effective way to remove antibiotics [22, 23].

Two antibiotics are investigated in this study: sulfamethazine and oxytetracycline. Sulfamethazine ($C_{12}H_{14}N_4O_2S$) is an antibiotic used to treat bronchitis, prostatitis and urinary tract infections. In laboratory, it is used in disposition and depletion kinetic studies, and to develop detection techniques for quantification in fluids such as cows' milk, honey and swine urine. Sulfamethazine has high stability in water due to its complex molecular structure, which makes it difficult to remove by biological processes[24].

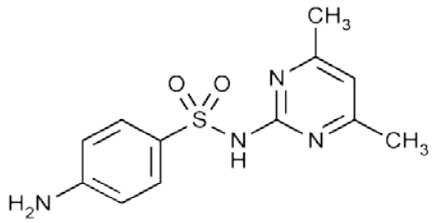

Figure 3.5- Sulfamethazine structure

Oxytetracycline ($C_{22}H_{24}N_2O_9$) is a broad-spectrum antibiotic, active against a wide variety of bacteria. It is used to treat infections caused by Chlamydia and infections caused by Mycoplasma organisms (e.g. pneumonia). It is also used to treat acne, due to its activity against the bacteria on the skin that cause acne. Oxytetracycline is commonly used in cattle farms for animal growth and disease prevention [25].

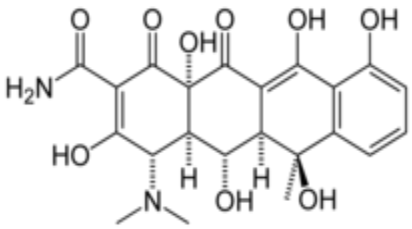

Figure 3.6- Oxytetracycline structure

3.4 Ferroxane derived ceramic membranes

Membrane technology has been extensively researched due to its high efficiency in removing small contaminates. The treatment process is mostly physical in which contaminants and colloids are trapped in the small pore spaces of the ceramic membranes. The benefits of ceramic membranes include high mechanical strength, high chemical compatibility, high flux, long operational life, high thermal stability, high hydrophilicity, and potentially lower life cycle cost due to the ease of operation, minimal maintenance, minimal pretreatment and low chemical and energy demands. The only potential limitation of ceramic membranes is the high capital cost [26-28].

In multiple studies, iron oxides have been coated on the surface of ceramics to improve treatment efficiency. An improvement in NOM removal was detected by the adsorption process; however, the resulting long-term fouling was a concern [29-31]. In addition, the typical synthesis process of iron oxides produces many environmental pollutants due to the shape-forming step, which uses a number of binders and solvents (often chlorinated, such as 1,1,1-trichloroethyline[32]) that are potentially toxic.

Ferroxane, a novel iron oxide nanoparticle that is synthesized through reacting lepidocrocite and acetic acid, is proposed in this research as an alternative to traditional iron oxides. The advantage of using ferroxane is that it is produced in an environmentally benign matter; no solvents or binders are necessary; hence no toxic byproducts are produced. Furthermore, ferroxane nanoparticles are produced in an aqueous solution at 70 C^o, which makes it more economical compared to other methods of producing iron oxides that typically require temperatures over 450 C^o[4, 30].

In previous studies, ferroxane coated ceramic membranes were proven to be effective in the removal of arsenic[31] and viruses[33] through adsorption processes. The potential catalytic capabilities of the ferroxane-derived membranes need to be further investigated, but they could be useful in degrading recalcitrant organics and non-biodegradable contaminants, such as pharmaceuticals.

3.5 Fenton Process

The Fenton process is an advanced oxidation process (AOP) typically used in wastewater treatment plants. Traditional Fenton consists of a reaction between Ferrous/ferric ions and H_2O_2 to generate **OH** radicals that could degrade contaminates[34]. The detailed Fenton process is shown below (Eq. 1-6). Ferrous ions initiate the decomposition of hydrogen peroxide, which oxidizes Fe(II) to Fe(III) in acidic conditions, forming the highly oxidant hydroxyl radical (Eq.1). Next, Fe (III) is reduced back to Fe(II) and hydroperoxyl radicals are produced (Eq. 2-3). Hydroxyl radicals can be scavenged by Fe(II) (Eq. 4) or H_2O_2 (Eq. 5). However, the reaction rate is much higher for Eq.(4), hence if the concentration

of iron is sufficiently high, Eq.(5) is negligible. Contaminants are then oxidized by the radical species formed according to Eq.(6)[35].

$Fe(II) + H_2O_2 \rightarrow Fe(III) + \mathbf{OH} + OH^-$	$k = 70\ M^{-1} s^{-1}$	Eq. (1)
$Fe(III) + H_2O_2 \rightarrow Fe(II) + \mathbf{HO_2} + H^+$	$k = 0.002\text{-}0.01\ M^{-1} s^{-1}$	Eq. (2)
$Fe(III) + \mathbf{O_2^-} \rightarrow Fe(II) + O_2$	$k = 1.2 \times 10^{-6}\ M^{-1} s^{-1}$	Eq. (3)
$Fe(II) + \mathbf{OH} \rightarrow OH^- + Fe(III)$	$k = 3.2 \times 10^{8}\ M^{-1} s^{-1}$	Eq. (4)
$H_2O_2 + \mathbf{OH} \rightarrow \mathbf{HO_2} + H_2O$	$k = 3.3 \times 10^{7}\ M^{-1} s^{-1}$	Eq. (5)
$\mathbf{OH}$ + organics → byproducts + $H_2O + CO_2$		Eq. (6)

(**Bold** fonts denote radical species)

Over the years, Fenton reactions have been extensively researched, and it has been proven experimentally that they are effective in the oxidation of organics[36-39], pesticides[40-43], dyes[44, 45], and pharmaceuticals[34, 46]. The process may initiate with either Fe(II) or Fe(III); however, the oxidation reaction of Fe(II) is much faster than the reduction of Fe(III), and therefore the initial organic degradation rate is slower when Fe(III) is the source of Fe[47]. Traditional Fenton reactions are performed under acidic conditions, with pH levels between 2 and 4—the optimum level being 3—and without the use of UV irradiation. This process is called Homogenous Dark Fenton[48].

The above-described process can be significantly accelerated by irradiance with UV and visible light; this process is called Homogenous Photo Fenton[36]. The UV light induces reaction 2 to generate more Fe(II) and **OH** radicals, resulting in the enhancement of the overall process[40]. Moreover, photo-Fenton processes are active at a pH near neutral due to their ability to break ferric complexes formed between the Fe(III) ions and the partially oxidized organics (ligands) in solution. However, as the organic ligands become degraded in the process, $Fe(OH)_3$ precipitate will be produced. Similarly to the dark

Fenton process, sludge is expected to be generated as a by-product of the oxidation, and a separation unit following the Fenton process is required[49].

This downside is overcome in the heterogeneous Fenton process. The mechanism involved has not been completely identified, but the following reaction path has been suggested:

$\equiv Fe(III)\text{-}OH + H_2O_2 \rightarrow \equiv Fe(III)\text{-}OH\text{-}H_2O_2$ Eq. (7)

$\equiv Fe(III)\text{-}OH\text{-}H_2O_2 \rightarrow \equiv Fe(II) + H_2O + \mathbf{HO_2}$ Eq. (8)

$\equiv Fe(II) + H_2O_2 \rightarrow \equiv Fe(III)\text{-}OH + \mathbf{OH}$ Eq. (9)

$\equiv Fe(III)\text{-}OH + \mathbf{HO_2} / \mathbf{O_2^-} \rightarrow \equiv Fe(II) + H_2O / OH^- + O_2$ Eq. (10)

where ≡ Fe(X)-OH are iron oxide surface sites

In acidic conditions, homogenous Fenton reactions rely on the dissolved iron species; however, in neutral conditions, heterogeneous Fenton reactions rely on the surface area of the precipitated ferric ions[50]. The heterogeneous process has several advantages over the homogeneous Fenton process: (a) the iron catalyst can be reused indefinitely since it can easily be removed from the treated water by sedimentation; (b) the process can be efficiently performed at neutral or slightly basic pH levels; (c) the catalyst can be fixed into a solid, avoiding the need for the separation step. Similar to the homogeneous Fenton process, the reaction rates can be enhanced by irradiation with UV light ($\lambda < 365$ nm)[44, 51].

In previous studies, micro- or nano-sized iron particles were doped with other metals to enhance the catalytic activity for heterogeneous Fenton reactions[39, 46, 52-54]. Doped iron particles showed important increases in catalytic activity due to the higher reduction potential of metals, such as Mn and Co: H_2O_2 decomposition rate increased by

30%[54]:$Fe^{3+}+1e^- \rightarrow Fe^{2+}$, $E^0=0.77V$; $Co^{3+}+1e^- \rightarrow Co^{2+}$, $E^0=1.81V$; $Mn^{3+}+1e^- \rightarrow Mn^{2+}$, $E^0=1.49V$.

The use of Fenton reactions for the degradation of methylene blue and antibiotics has been researched in the past and up to 100% removal of contaminates has been achieved. However, most the methods that have been applied require low pH (2.5-3), and use iron oxide that has been synthesized using an environmentally harmful method that generates toxics[7, 55].

4 Materials and Methods

4.1 Materials Synthesis

4.1.1 Lepidocrocite Synthesis

According to published methods [56], lepidocrocite (γ-FeOOH) nanoparticles were synthesized from the oxidation of ferrous chloride ($FeCl_2$) under controlled pH conditions. Using the set up shown in figure 4.1, a 0.2M solution of iron(II) chloride tetrahydrate (99% Sigma, St. Louis, MO, USA) was prepared in 18mΩ water. Air was provided throughout the reaction by a diffuser. 0.1M NaOH (Acros, NJ, USA) solution was used to maintain the reaction pH between 6.7-6.9. while continuous mixed and aerated for 3 hours. The reaction was stopped when an orange precipitate was obtained. The orange particles were centrifuged for 8 minutes at 3,500rpm and the supernatant was discarded. The product was then purified: the precipitate was re-suspended and centrifuged 3 additional times to remove NaCl produced during the oxidation. The precipitate was finally dried at 50°C in a crystallization dish to yield lepidocrocite particles.

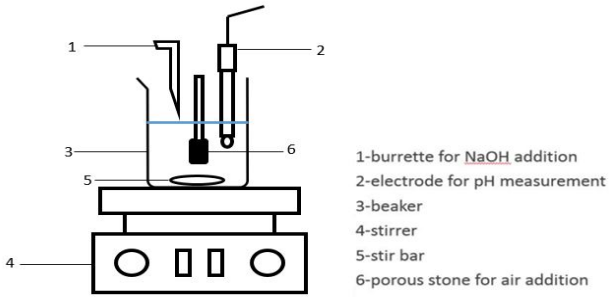

Figure 4.1- illustration of experimental set up for lepidocrocite synthesis

4.1.2 Ferroxane synthesis

Ferroxane nanoparticles were produced through reacting the synthesized lepidocrocite particles with acetic acid [30]. Briefly, 4g of lepidocrocite particles and 5 ml of glacial acetic acid (Fisher, Nazareth, PA, USA) were added to 100 ml of ultrapure water (18mΩ), to give a molar ratio of 2:1 (acetic acid to iron). The reaction was maintained at 70 C^{o} while continuously stirred for 3 hours. A reflux condenser was used to keep the acetic acid in the reaction. Finally, the suspension was centrifuged for 10 minutes at 3,700 rpm to remove unreacted lepidocrocite particles. The supernatant was collected and dried in the oven at 60°C.

4.1.3 Hematite

Hematite nanoparticles were prepared by sintering at a maximum temperature of 500 C the ferroxane nanoparticles according to the program described in Table 2 below. The sintering process was carried out using a high temperature furnace (Vulcan 3-550, Neytech, USA).

Table 4.1- Sintering process of ferroxane nanoparticles into hematite

Rate of temperature increase (°C/min)	Temperature Range (°C)	Hold time at maximum temperature (hours)
1.0	0 - 150	2
1.0	150 - 350	3
1.0	350 - 500	4

4.1.4 Ceramic membranes synthesis

Ferroxane nanoparticles were deposited on the surface of the ceramic membrane by using vacuum filtration. In this process, 150 ml of a 140 mg/l ferroxane solution was filtered through a ceramic membrane in a Buchner funnel. The ferroxane nanoparticles were trapped on the surface of the ceramic, while the water was drawn by a vacuum through the funnel to the bottom of the flask, as shown in figure 4.2 below:

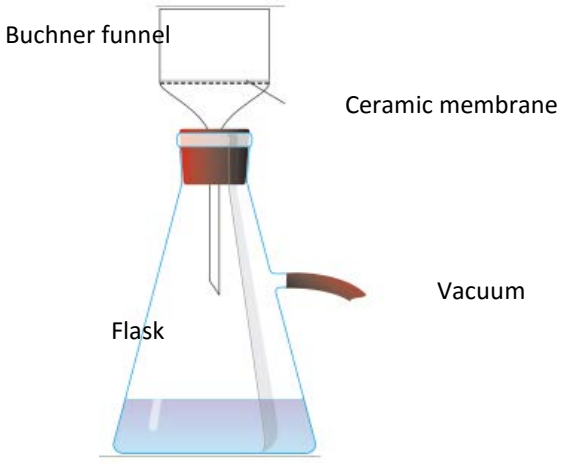

Figure 4.2- Vacuum filtration for deposition of ferroxane nanoparticles on the surface of ceramics

The ceramic membranes were allowed to dry at room temperature for 24 hours before sintering according to the program shown in Table 4.1.

4.1.5 Doped metals ferroxane synthesis

Ferroxane nanoparticles were doped with Mn and Co following a proposed fabrication route which is based on mixed metal alumina synthesis [57] and previous experiments results [58]. The elements were selected based on their reduction potential between their

cationic oxidation states compared to that of iron: $Fe^{3+}+1e^- \rightarrow Fe^{2+}$, $E^0=0.77V$; $Co^{3+}+1e^- \rightarrow Co^{2+}$, $E^0=1.81V$; $Mn^{3+}+1e^- \rightarrow Mn^{2+}$, $E^0=1.49V$ [59].

For each dopant, synthesis at iron to metal molar ratios of 2:1, 4:1, and 10:1 were considered to determine the degree of substitution attainable by this method. The synthesis of doped ferroxane nanoparticles was conducted as explained below (all chemicals are available through Sigma-Aldrich). Ferroxane nanoparticles (1 g.) were suspended in 200 ml of ultrapure water (18 MΩ) and mixed in a solution of the corresponding concentration of manganese(II) acetylacetonate or cobalt(II) acetylacetonate. The reaction was stirred for 24 hours at room temperature and then centrifuged at 9500 rpm for 8 minutes to separate the solid. The doped-ferroxane nanoparticles were dried in the oven at 50°C and stored for future use.

4.2 Materials characterization

4.2.1 X-Ray Diffraction (Ultima IV X-Ray Diffractometer—Rigaku, Japan)

X-ray diffraction (XRD) relies on the dual wave/particle nature of X-rays to obtain information about the structure of crystalline materials. A primary use of the technique is the identification and characterization of compounds based on their diffraction pattern.

XRD is based on the scattering of the x-rays after hitting the structure's surface as well as the constructive interference of the waves that are in phase. Based on the scattering and the dispersion in space, the crystalline structure will display a certain signature that is unique. The interaction between the rays and the sample create diffracted rays, which can be described by Bragg's law:

$$n\lambda = 2d\ sin\Theta \quad \text{(Equation 4.1)}$$

where n is the order of diffraction, λ is the wave length of the x-ray beam, d is the inter-planar distance, and 2Θ is the angle of diffraction [60].

In this work, XRD was used to analyze lepidocrocite, ferroxane, and hematite in order to obtain the crystallography of the sample; thus, confirm the identity.

4.2.2 Dynamic Light Scattering (Zetasizer Nano ZS ZEN3600—Malvern, UK)

Dynamic light scattering (DLS) is technique used to determine the size distribution profile of small particles in suspension. Using a laser, a monochromatic light beam is shinned onto a solution with spherical particles. The beam hits the surface of the particles and scatters, which also changes the wavelength of the incoming light. The scattered light is then collected by a photomultiplier. The resultant intensity that can be observed is the vectorial sum of the scattering from each of the particles in the suspension.

The intensity of the scattered lights fluctuates due to Brownian motion of the particles. These fluctuations are correlated, and an auto-correlation function for the intensity of scattered light can quantify this correlation [61]:

$$G(\tau) = \langle I_s(t)I_s(t+\tau)\rangle \quad \text{(Equation 4.2)}$$

where I_s is the scattering intensity, t is time, and τ is the time shift. The usefulness if $G(\tau)$ is that it can be directly related to the particle diffusivity for a dispersion of monodisperse particles [61]:

$$G(\tau) = A_0 + Ae^{-\Gamma\tau} \quad \text{(Equation 4.3)}$$

where A_0 is the background signal, A is an instrument constant, and Γ is the decay constant. The measured decay constant gives the particle diffusion coefficient, according to the equation [61]:

$$\Gamma = Q^2 D \qquad \text{(Equation 4.4)}$$

where Q is the magnitude of the scattering wave vector, and D is the particle diffusion coefficient. When the particle diffusion coefficient is found, particle radius can be found, assuming spherical shape [61]:

$$a = \frac{kT}{6\pi\mu D} \qquad \text{(Equation 4.5)}$$

where a is particle radius, k is the Boltzmann constant, and T is temperature.

In this work, DLS was used to analyze the size of the ferroxane nanoparticles and metal doped ferroxane nanoparticles. Suspensions of the materials (100 mg/l) were prepared using ultrapure water (18mΩ). Then, 1 mL of the solutions were put into a plastic cuvette for analysis. The refractive index for iron oxide is 2.9 and the absorption is 0.3.

4.2.3 Zeta Potential (Zetasizer Nano ZS ZEN3600—Malvern, UK)

Zeta Potential analysis is a method that defines the surface charge of nanoparticles suspended in liquid media. Generally, most nanoparticles have a surface charge that attracts opposite charged ions to the nanoparticle surface, resulting in forming a tiny layer around the nanoparticles. This layer of ions travels with each nanoparticle as it diffuses throughout the solution. A stable entity is formed between the ions and particles by a notional boundary within the diffused layer. Ions within this boundary move with the particle as it moves, but any ions beyond the boundary do not travel with the particle.

This boundary is called the surface of hydrodynamic shear or slipping plane. The electric potential at this boundary is known as the Zeta potential of the particles, and has values that typically range from +100 mV to -100 mV. The magnitude of the zeta potential is predictive of the colloidal stability. Nanoparticles with Zeta Potential values greater than +30 mV or less than -30 mV typically have high degrees of stability. Dispersions with a low zeta potential value will eventually aggregate due to Van Der Waal inter-particle attractions.

In this work, zeta potential measurements are used to obtain the point of zero charge of ferroxane and metal doped ferroxane.

4.2.4 Surface Area (Coulter SA3100—Beckman Coulter, USA)

Brunauer, Emmett, and Teller (BET) method is commonly used to determine the surface area of solid particles from Nitrogen gas adsorption on the surface of the solid. Then the surface area is estimated using the Langmuir model: a known amount of gas is used to form a monolayer of gas molecules on a solid, and the occupied area of these adsorbed molecules makes it possible to estimate the area of the solid.

Before the specific surface area of the sample can be determined, it is necessary to remove gases and vapors that may have become physically adsorbed onto the surface after the syntheses and during handling and storage. This process is called outgassing, and generally involves heating the samples for a period of time in a flow of helium or nitrogen.

In this work, the BET specific surface area was measured for ferroxane, hematite, and metal-doped ferroxane nanoparticles. Each sample was outgassed with a helium purge for

180 minutes at 300°C prior to acquiring the nitrogen adsorption isotherm. Nitrogen was used as the adsorbing gas. [62]

4.2.5 Scanning Electron Microscopy (Quanta 650 FEG—FEI, USA)

The scanning electron microscope (SEM) is a characterization technique used to view and image small-scale materials. SEM uses a focused beam of high-energy electrons to generate a variety of signals at the surface of solid specimens. The signals emitted by the electrons and radiation that result from the impact are collected by a detector and amplified [63]. The result is an enlarged topographic image of the sample. The signals derived from electron-sample interactions reveal information about the sample's texture.

In addition, the SEM is also capable of performing analyses on selected point locations on the sample. This allows the users to semi-quanitiavly determine the chemical composition of a sample, using Energy-Dispersive X-Ray Spectroscopy (EDS). An EDS detector separates the x-rays of different elements into an energy spectrum, and EDS system software is used to determine the type of specific elements in the sample [63].

SEM produces high-resolution images (10 to 100,000 times magnification). In this work, SEM is used to determine the crystalline structure of hematite and metal-doped ferroxane nanoparticles. In addition, EDS is used to confirm the success of the doping process by showing the existence of Mn and Co in the structure of ferroxane. In order to test the samples, the suspended particles were fixed on metal supports by using carbon tape.

4.2.6 Spectrophotometer

UV-visible spectrophotometry is a technique that can be applied to the measurement of concentrations of dissolved compounds, if they absorb light at any wavelength within the UV or visible spectrum. Spectrophotometer measures the intensity of a light beam before and after it passes through a sample, and therefore can determine how much light was absorbed by the chemical compound. Using a calibration curve, this adsorption number can be converted into concentration in solution. Spectrophotometers use Lambert-Beer law. Beer-Lambert Law (also known as Beer's Law) states that there is a linear relationship between the absorbance and the concentration of a sample. Beer's Law is written as:

$$A=\varepsilon lc \quad \text{(Equation 4.6)}$$

Where A is the measure of absorbance (no units), ε is the molar extinction coefficient or molar absorptivity (or absorption coefficient),l is the path length, and c is the concentration.

In this work, spectrophotometer is used to measure the concentration of methylene blue in samples taken at different stages during the Fenton reaction experiments.

4.2.7 High Pressure Liquid Chromatograph

High-pressure liquid chromatography (HPLC) is an analytical technique used to separate, identify, and quantify different components in a mixture. A sample mixture or analyte in a solvent (known as the mobile phase) is pumped at high pressure through a column with chromatographic packing material (stationary phase). The sample is carried by a moving

carrier gas stream of helium or nitrogen. Each component in the sample interacts slightly differently with the packing material, causing different flow rates for the different components, and leading to the separation of the components as they flow out the column. The time at which a specific analyte emerges from the column is called its retention time. The retention time measured under particular conditions is an identifying characteristic of a given analyte.

In this work, HPLC is used to test the degradation rates of Sulfamethazine and Oxytetracycline during Fenton reactions, and the plot of concentration (C/C_0) versus reaction time (t) will be obtained. The concentrations of oxytetracycline and sulfamethazine were determined with aShimadzu SCL-10Avp HPLC system with photodiode array detector. The compounds were separated by a Phenomenex (Torrance, CA) Kinetex C18 (100mm x 4.6 mm; 2.6 µm particle size) reverse-phase column. The mobile phase consisted of 0.1% phosphoric acid in water (A) and 100% acetonitrile (B). The gradient conditions were 0–0.5 min, 2% B; 0.5–7 min, 2–80% (linear gradient) B; 7.0–9.0 min, 80–98% (linear gradient) B; 9.0–10.0 min (linear gradient), 2% B; 10.0–15.0 min, 2% B at a flow rate of 0.5 ml/min. The Oxytetracycline and Sulfamethazine were detected and quantified with UV 254 nm.

4.3 Experimental methods

4.3.1. Reactor Set up

Catalytic activity of the prepared samples will be compared in a first instance by their ability to decompose hydrogen peroxide, the main component in Fenton reactions. All reactions take place in a 1000 ml glass beaker. Different concentrations of hematite ,

H_2O_2, methylene blue, and/or UV_{365} light are added to 200 ml of water, and the beaker is set on top of a magnetic stirrer plate in order keep the solution homogenous. Samples are taken every 10 minutes for the first hour, then every 30 minutes afterwards. The set-up is shown in figure 4.3.

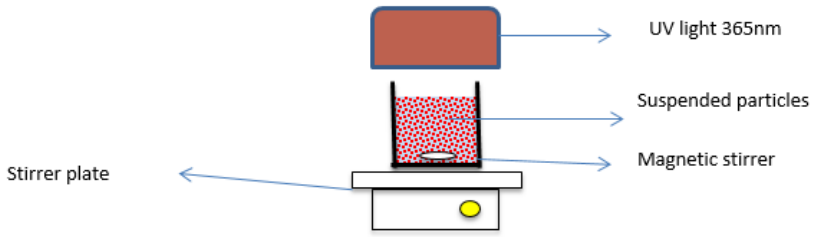

Figure 4.3- reactor set up

4.3.2 Effect of H_2O_2 concentration

Optimization of H_2O_2 concentration was performed by adding 2 g/l of hematite, 10 ppm of methylene blue, and UV365 to the reactor while varying the concentration of H_2O_2. Concentrations tested were 40, 150, 300, and 400 mM. The pH of the solution was kept constant at 7.6. The concentration of methylene blue was monitored using a spectrophotometer over the course of 5 hours.

4.3. 3 Effect of UV irradiation

To test the effect of UV irradiation on the degradation of methylene blue, 10 ppm of methylene blue was added to the reactor, and UV at wavelength of 365nm was set on top of the reactor as shown in figure 3.1. Samples were taken to measure the concentration of methylene blue over the course of 5 hours using a spectrophotometer. The pH of the solution stayed constant at 7.6.

4.3. 4 Effect of hematite concentration and system optimization

The effect of hematite concentration on the decomposition of hydrogen peroxide and degradation of methylene blue is tested by adding 400 mM of H_2O_2 and UV_{365} to the reactor, while varying the concentration of hematite. Hematite concentrations of 2, 4, 6, and 8 g/l are tested. The pH of the solution kept constant at 7.6. Methylene blue concentration is measured by using a spectrophotometer over the course of 5 hours.

The adsorption capability of hematite is tested by adding 8 g/l of hematite and 10 ppm of methylene blue to the reactor. The concentration of methylene blue over time is measured by using a spectrophotometer at 665 nm. Samples are taken over the course of 5 hours.

The effect of hematite concentration on the decomposition of H_2O_2 without the use of UV irradiation is measured by the adding 400 mM of H_2O_2, 8g/l of hematite, and 10 ppm of methylene blue to the reactor. The concentration of methylene blue is measured over the course of 5 hours by using a spectrophotometer.

4.3.5 Effect of Mn, Co doped ferroxane

The effect of Mn, Co doped ferroxane, iron to metal ratio 2:1, concentration on the decomposition of hydrogen peroxide and degradation of methylene blue is tested by adding 8 g/l of catalyst, 400 mM of H_2O_2 , 10 ppm methylene blue, and UV_{365} to the reactor. The pH of the solution kept constant at 7.6. Methylene blue concentration is measured by using a spectrophotometer over the course of 2 hours.

4.4.6 Effect of hematite on antibiotics degradation

The effect of hematite on the degradation of Sulfamethazine and Oxytetracycline is tested by adding 8 g/l of hematite, 1 ppm antibiotics, 400 mM of H_2O_2 and UV_{365} to the reactor. The pH of the solution stayed constant at 7.6. Samples were taken every 10 minutes for the first hour, then every 30 minutes for the second hour. Antibiotics concentration were measured using HPLC methods described earlier.

5 RESULTS AND DISCUSSIONS

5.1 Materials Characterization

5.1.1 X-Ray Diffraction

X-ray diffraction was conducted on ferroxane, magnetite, and hematite to confirm their identity. Results are shown in figures 5.1-5.3. Figure 5.1 (is the XRD diffractogram for ferroxane. As ferroxanes are a novel material, there is not a typical XRD diffractogram in the database that the X-Ray diffractometer used in this work references; however, ferroxanes are very similar in structure to lepidocrocite, so the blue lines in indicate typical peaks for lepidocrocite. This result was expected; the synthesis of ferroxane produces a reduction in size of the iron oxide particles, and should not alter its crystalline structure lepidocrocite.

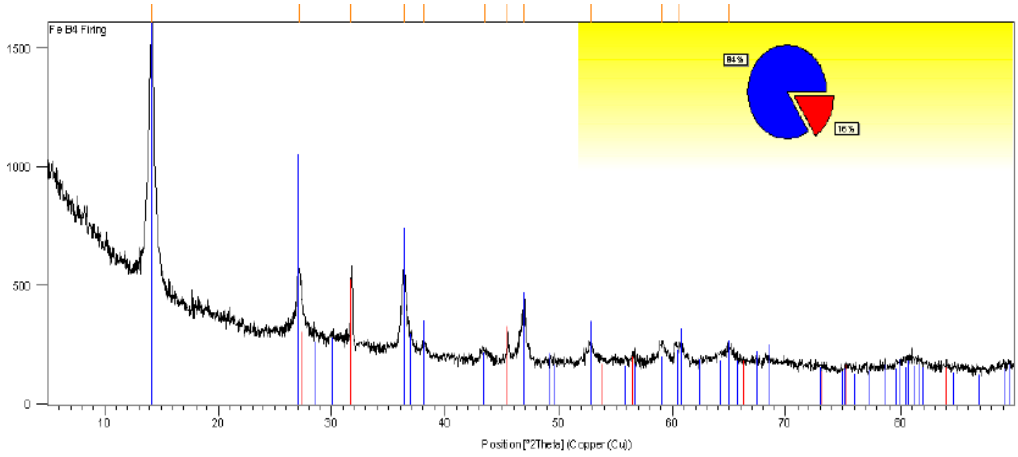

Figure 5.1- X-Ray diffraction for ferroxane

Figure 5.2 is the XRD diffractogram for magnetite. Magnetite was prepared by sintering ferroxane at 400 C°. The diffractogram confirms that sintering ferroxane at 400 C° produces magnetite.

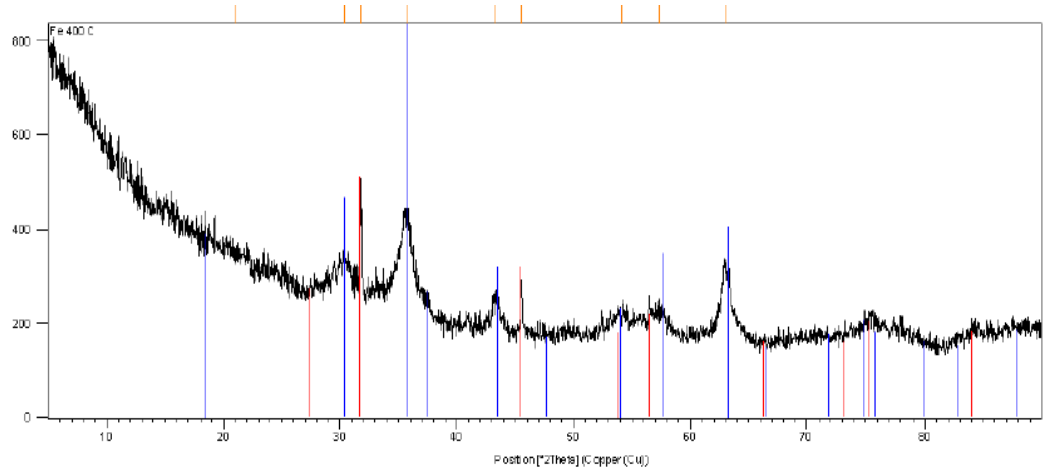

Figure 5.2- X-Ray diffraction for magnetite

Figure 5.3 is the XRD diffractogram for hematite. Hematite was prepared by sintering ferroxane at 500 C°. The results confirm that the sintering process is successful at producing hematite. It can be seen that the peaks are more organized and sharp for hematite, while they are wide and less uniform for magnetite, which is an indication of a closely packed material.

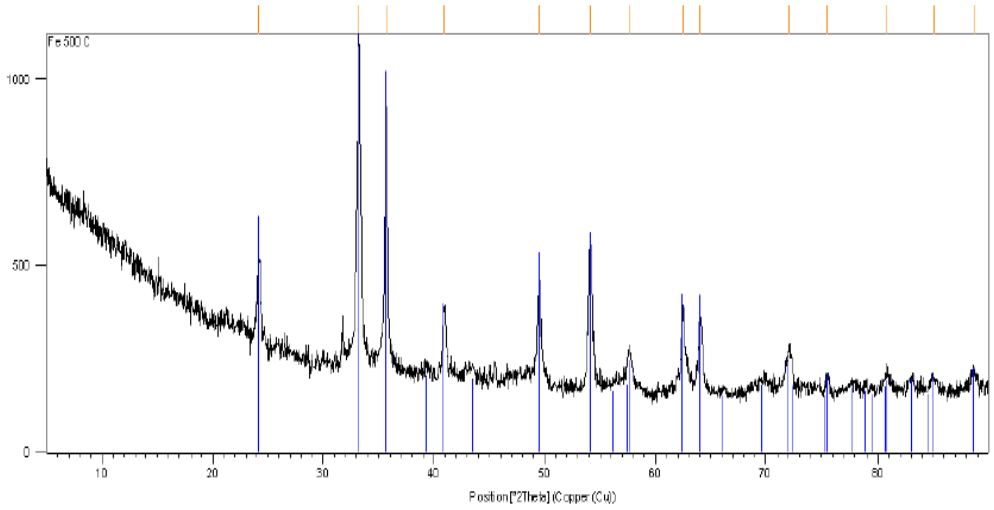

Figure 5.3- X-Ray diffraction for hematite

5.1.2 Scanning Electron Microscopy (SEM) and Energy-Dispersive X-Ray Spectroscopy (EDS)

SEM images were taken for the ferroxane and metal doped ferroxane nanoparticles to observe and compare the surface morphology. However, the pictures were not clear enough to be presented in this work due to the conductivity of the particles. On the other hand, there was no difference between the morphology of ferroxane and the doped ferroxane. This was expected as the doped metals should not alter the structure of iron oxide.

EDS analysis was performed to confirm the existence of Mn and Co in doped samples. Results are shown in figures 5.4-5.6. The results in figure 5.4 show the existence of iron in the sample. In addition, O_2, Na, and Cl peaks exist in the sample. That's expected as NaCl is used in the synthesis of lepidocrocite (see methodology section), and oxygen is part of the iron oxide structure (Fe_2O_3).

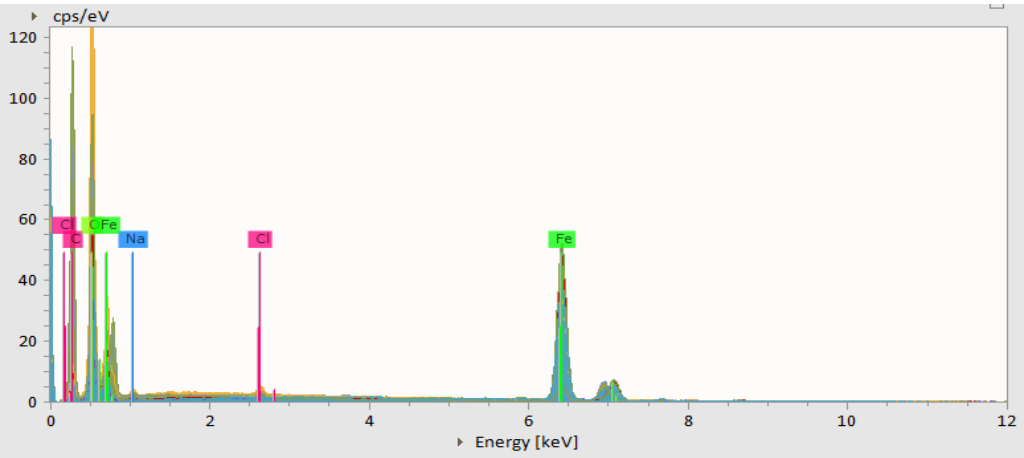

Figure 5.4- Energy-Dispersive X-Ray Spectroscopy (EDS) of Ferroxane

Figures 5.5 and 5.6 show the EDS analysis of Mn doped ferroxane and Co doped ferroxane, respectively, at molar ratios of 2:1. The analysis shows the existence of Mn and Co in the samples; hence, this indicates that the doping process is successful.

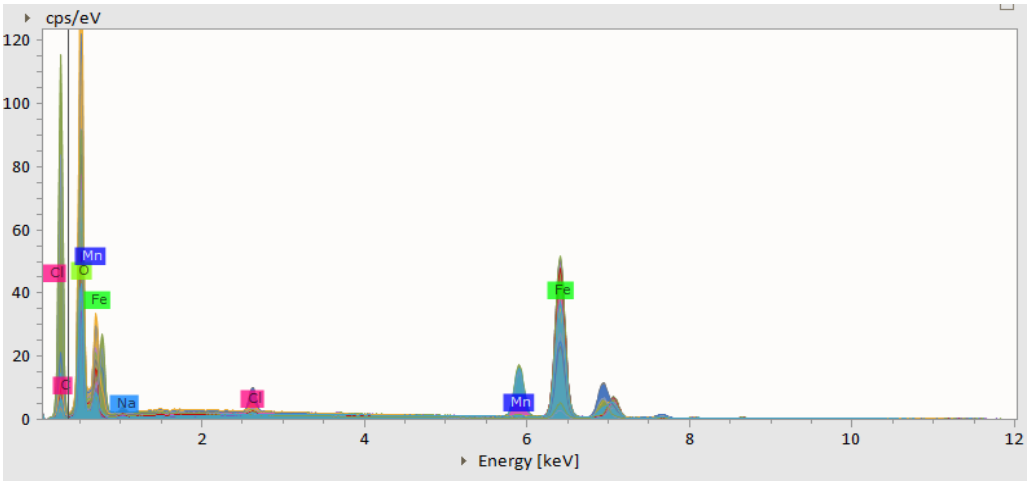

Figure 5.5- Energy-Dispersive X-Ray Spectroscopy (EDS) of Mn doped ferroxane at 2:1 ratio

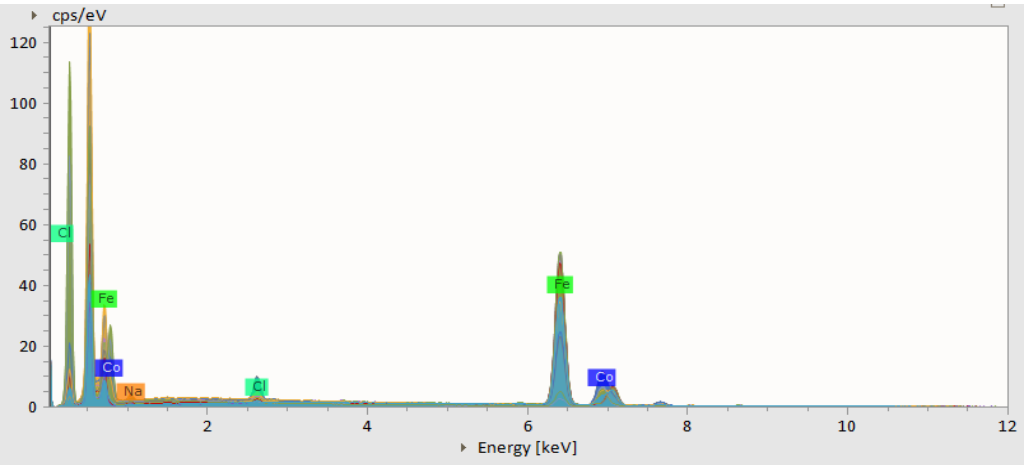

Figure 5.6- Energy-Dispersive X-Ray Spectroscopy (EDS) of Co doped ferroxane at 2:1 ratio

5.1.3 Surface Charge (Zeta Potential)

The surface charge of ferroxane, cobalt doped ferroxane, and manganese doped ferroxane at molar ratios of Fe to metal of 10:1, 4:1, 2:1 at varying pH levels are shown in figures 5.7-5.8.

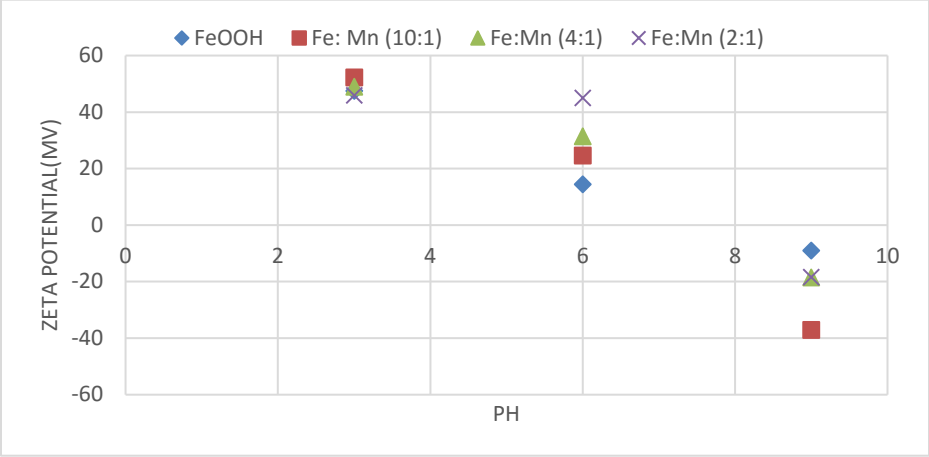

Figure 5.7- zeta potential measurements at varying pH for ferroxane and Mn doped ferroxane at molar ratios of Fe:Metal of 10:1, 4:1, and 2:1

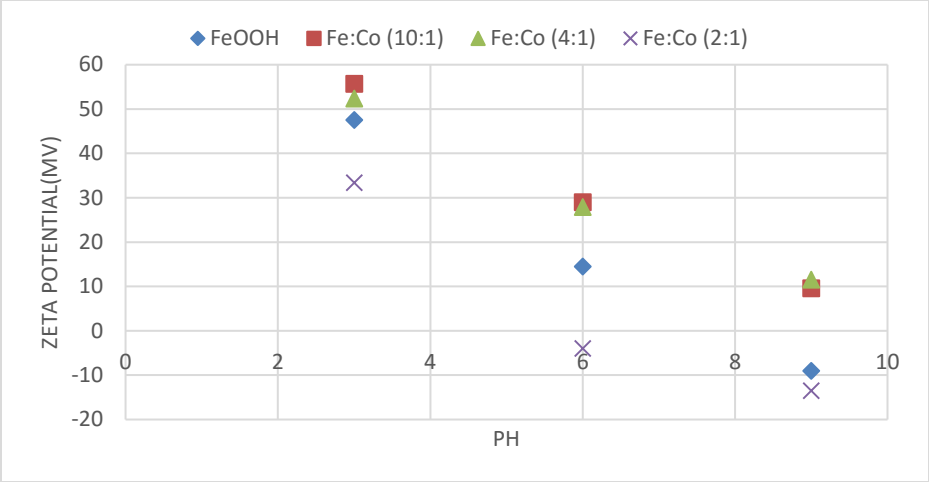

Figure 5.8- zeta potential measurements at varying pH for ferroxane and Co doped ferroxane at molar ratios of Fe:Metal of 10:1, 4:1, and 2:1

As shown in figures, the surface charge of ferroxane becomes less positive as the pH increases, reaching a point of zero charge (pzc) at pH of 7.8. In literature, lepidocrocite has a point of zero charge (pzc) ranging from pH 6.7 to pH 7.5; thus, the findings in this work regarding the zeta potential of ferroxane are accurate. At pH higher than 7.8, ferroxane has a negative surface charge.

Figure 5.7 is the surface charge measurements for Mn doped ferroxane. At pH 6, the surface charge of the doped particles becomes more positive as the amount of Mn doped increases. In addition, the pzc of the doped particles differ from ferroxane particles: 7.2, 7.9, and 8.2 for 10:1, 4:1, and 2:1 ratio respectively. This indicates that the new synthesized nanoparticles differ from the original material (ferroxane), therefore, confirming the success of the doping process.

Similar results can be seen with Co doped ferroxane in figure 5.8; however, there's no uniform pattern of surface charge change with increasing the amount of Co doped. The

doped nanoparticles have a pzc at pH 5.7 for 2:1 ratio, while the pzc was not reached for the other ratios.

Molar ratios of 2:1 will be used for all further experiments as the pzc is reached for Co doped ferroxane at that ratio, and to ensure the availability of high enough metal concentration to impact the degradation experiments.

The pzc is critical in this research as it indicates the operating pH values of the reactor. Methylene blue is a positive organic; therefore, in order to have electrostatic attraction (van der Waals attraction) in the reaction, the iron surface charge has to be negative. The negatively charged iron particles attract the positively charged methylene blue, where it could be removed by adsorption or removed by **OH** radicals generated from H_2O_2 decomposition.

5.1.4 Dynamic Light Scattering (DLS)

The particle size of ferroxane, cobalt doped ferroxane, and manganese doped ferroxane at molar ratios of Fe to metal of 10:1, 4:1, 2:1 at varying pH levels are shown in figure 5.9-5.10.

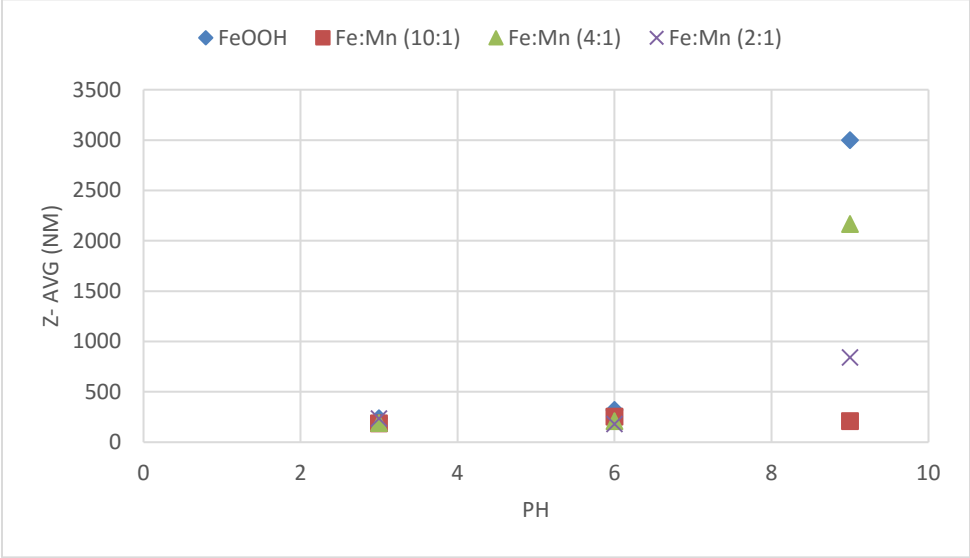

Figure 5.9- zeta potential measurements at varying pH for ferroxane and Mn doped ferroxane at molar ratios of Fe:Metal of 10:1, 4:1, and 2:1

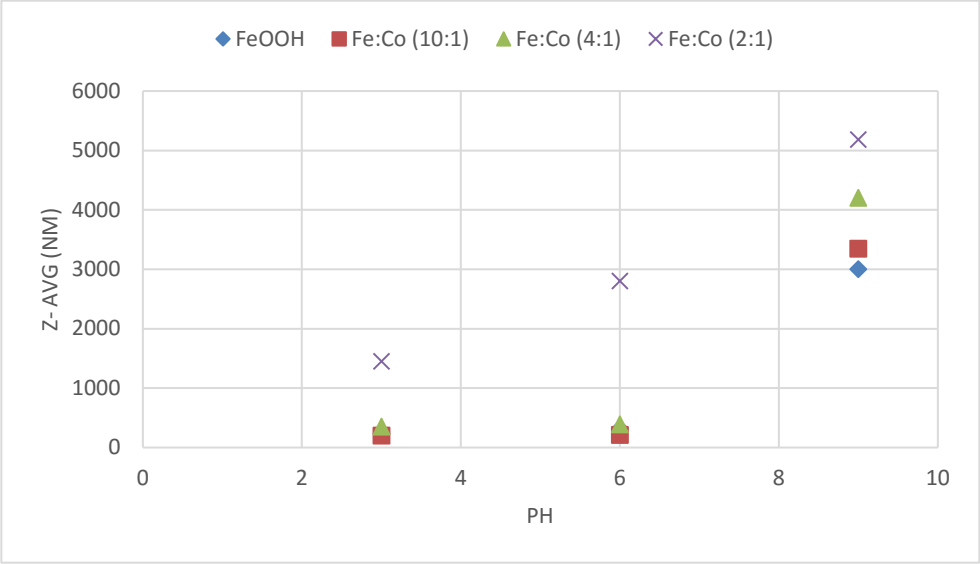

Figure 5.10- zeta potential measurements at varying pH for ferroxane and Co doped ferroxane at molar ratios of Fe:Metal of 10:1, 4:1, and 2:1

The results show that the size of ferroxane nanoparticles at pH 6 is 230 nm. At pH 3 ferroxane has particle size of 190 nm. The decrease in size could be caused by the particles dissolving at low pH. At pH 9, ferroxane particles have an average size of 3000 nm. The increase in size is caused by particles aggregation at high pH.

Figure 5.9 shows that average particle size of Mn doped ferroxane particles are around 230 nm at pH 6 for all ratios. At pH 9, the particles seem to aggregate rapidly and the size increases.

Similar results are obtained for Co doped ferroxane in figure 5.10. Average particle size increases as pH and amount of Co doped increases. However, at 2:1 ratio, particle size is larger than other ratios.

All particles show significant aggregation at pH values higher than 8; therefore, pH values above 8 will not be considered to avoid settlement

5.1.5 Surface Area

The surface area for nanostructured hematite was determined by using the Brunnauer, Emmett, and Teller method for specific surface area analysis. Determining surface area is important as it provides information as to the number of adsorption sites available, and also the amount of surface available for potential catalytic interactions. Table 5.1 summarizes the surface area for ferroxane nanostructured hematite used in this work.

Table 5.1--BET surface area for ferroxane and Hematite

Material	**Specific surface area (m^2/g)**
Ferroxane	72.47 ± 2.01
Hematite	23.24 ± 3.5

These values are in agreement with the surface area of hematite that was reported by Cornell, surface area of hematite formed by dehydroxylation of lepidocrocite at temperature < 500 ºC ranges from 2-200 m^2/g [4]. In addition, De Angelis and Cortalezzi [64] reported a specific surface area for hematite of 41.88 ± 5.42 m^2/g. Higher surface area should allow for a greater number of adsorption sites, and greater adsorption.

The results show a decrease in surface area after converting ferroxane to hematite. This could be caused by the sintering process, as this compacts the materials and creates larger nanoparticles; hence, reducing the overall surface area.

5.2 Degradation Experiments

5.2.1 Methylene Blue Experiments

5.2.1.1 Effect of H_2O_2 concentration

Results from the H_2O_2 optimization experiment are shown in figure 5.11.

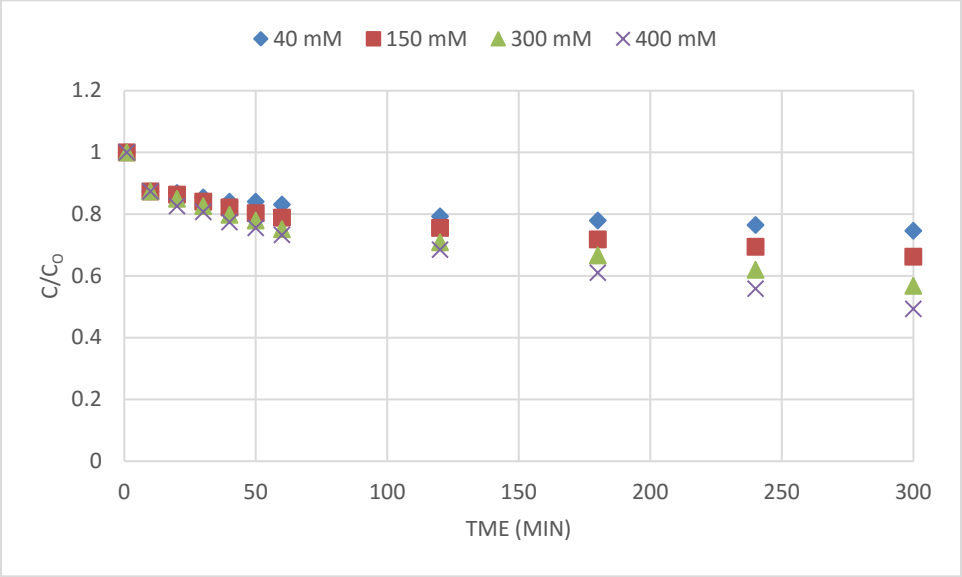

Figure 5.11- Effect of the concentration of H_2O_2 on the concentration of MB under the following conditions: 10 ppm MB, 2 g/l hematite, pH=7.6, UV light 365 nm.

As seen in figure 5.11, methylene blue concentration decreases as the concentration of H_2O_2 increases. That's due to the increase in the amount of hydroxyl radicals generated from the decomposition of H_2O_2. Therefore, 400 mM concentration of H_2O_2 is chosen for all experiments.

It's noteworthy that the addition of high concentrations of H_2O_2 could eventually slow down the degradation process instead of speeding it. That's due to the fact that the excess generated hydroxyl radicals are scavenged by H_2O_2 (as shown in reaction 5), causing a decrease in methylene blue degradation. In addition, adding higher concentrations of

H_2O_2 increases the cost of treatment, therefore, concentrations higher than 400 mM are not considered in this research.

5.2.1.2 Effect of hematite concentration and system optimization

The effect of hematite concentration on the degradation of methylene blue is shown in figure 5.12.

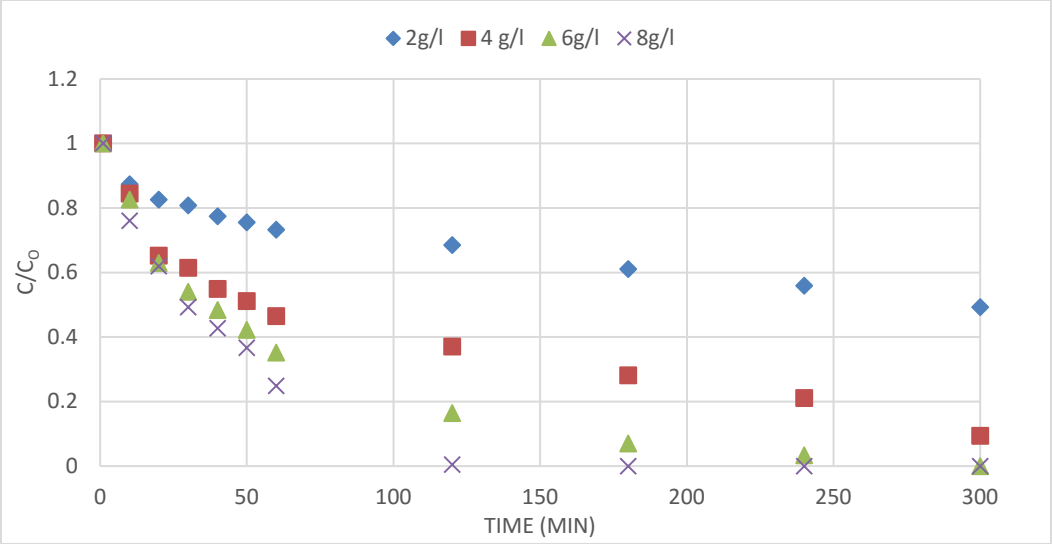

Figure 5.12- The effect of hematite concentration on the degradation of MB under the following conditions: 10 ppm MB, 400 mM H_2O_2, UV365, pH= 7.6.

As shown in figure 5.12, the degradation of methylene blue increases as the concentration of hematite increases. 100% degradation of methylene could be achieved within 2 hours of reaction if 8 g/l of hematite is used; however, using 6 g/l, 100% degradation is achieved after 5 hours of reaction. The addition of higher concentrations of hematite increases the available surface area of the catalyst that could react with H_2O_2 to generate hydroxyl radicals faster.

Reaction kinetics are important for Fenton reactions as the H_2O_2 will evaporate from the reaction at long hydraulic retention times (HRTs). In addition, HRTs higher than 2 hours

are generally considered unrealistic for water treatment processes. Therefore, a concentration of 8 g/l is used in this research.

The adsorption capability of hematite, and the degradation capability of hematite combined with H_2O_2 without the use of UV are tested. The results are shown in figure 5.13. In addition, figure 5.13 shows the degradation of methylene blue naturally without the addition of iron, H_2O_2, or UV. Also, the effect of UV irradiation by itself is shown in the figure as well.

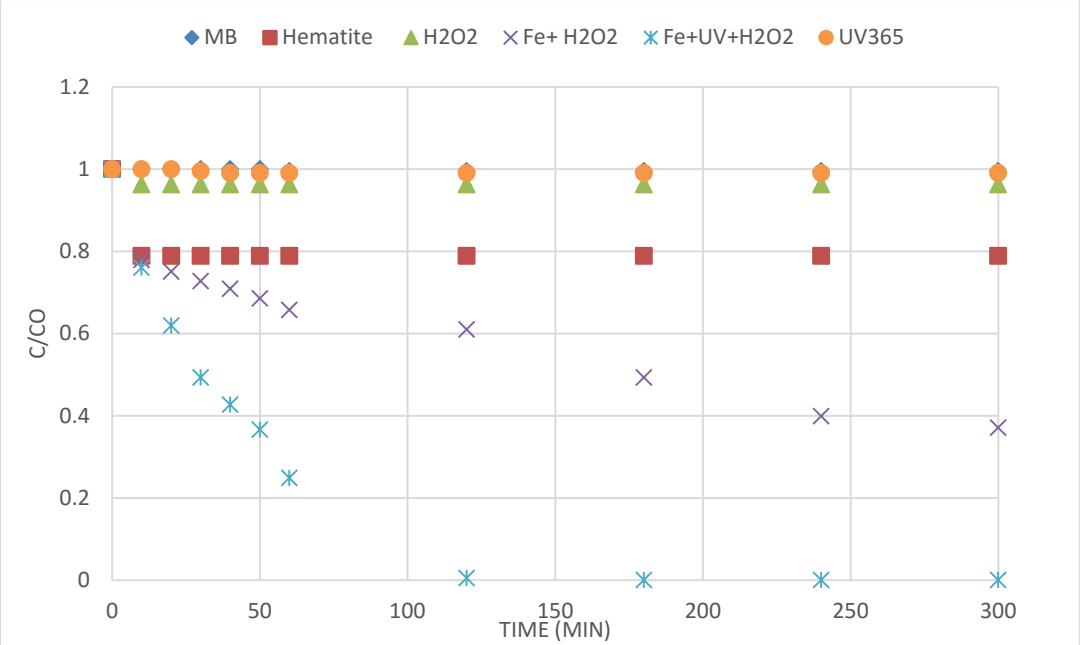

Figure 5.13- The degradation process of MB for the following experiments: MB alone (control sample), hematite alone, H_2O_2 alone, UV_{365} alone, hematite + H_2O_2, hematite + H_2O_2 + UV_{365}. The reaction conditions are: 10 ppm MB, 400 mM H_2O_2, 8 g/l hematite, pH= 7.6.

The results show that methylene blue does not degrade naturally, or even with the addition of UV_{365}, over the course of 5 hours. Also, the degradation of methylene blue by H_2O_2 alone over the course of 5 hours is negligible, about 4% degradation. That could be explained by the slow decomposition rate of H_2O_2 by itself.

As shown in the figure 5.13, hematite alone is capable of adsorbing 20% of the methylene blue concentration within the first 10 minutes of reaction. The adsorption is caused by the electrostatic attraction between the surface of the hematite particle (negatively charged at pH 7.6) and the positively charged methylene blue. Adsorption of methylene blue after 10 minutes is negligible due to decrease in the available surface area of hematite.

When Hematite and H_2O_2 are added to the reactor, about 61% removal of methylene blue occurs over the course of 5 hours. The catalytic activity caused by the iron surface is increasing the decomposition rate of H_2O_2, generating more **OH** radicals (as shown in Eqs. 7-10). Furthermore, as UV_{365} is added to the reaction, a 100% removal occurs over the course of 2 hours. This is caused by the UV light inducing reaction (8) to generate more Fe(II) and **OH** radicals. The results show promising capabilities of the photo induced heterogeneous Fenton process in degrading high concentrations of methylene blue.

5.2.1.3 Effect of Mn, Co doped ferroxane

To test the effect of Mn, Co doped ferroxane, at 2:1 molar ratio, on the degradation of methylene blue, the pH of each solution is changed to be close or higher than the PZC. For Co doped ferroxane and Hematite experiments, the pH is set at 7.6 since the PZC. For Mn doped ferroxane, the pH of the solution is set at 8.0, since the PZC for the nanoparticles is 8.2. Results of the experiments are shown in figure 5.14.

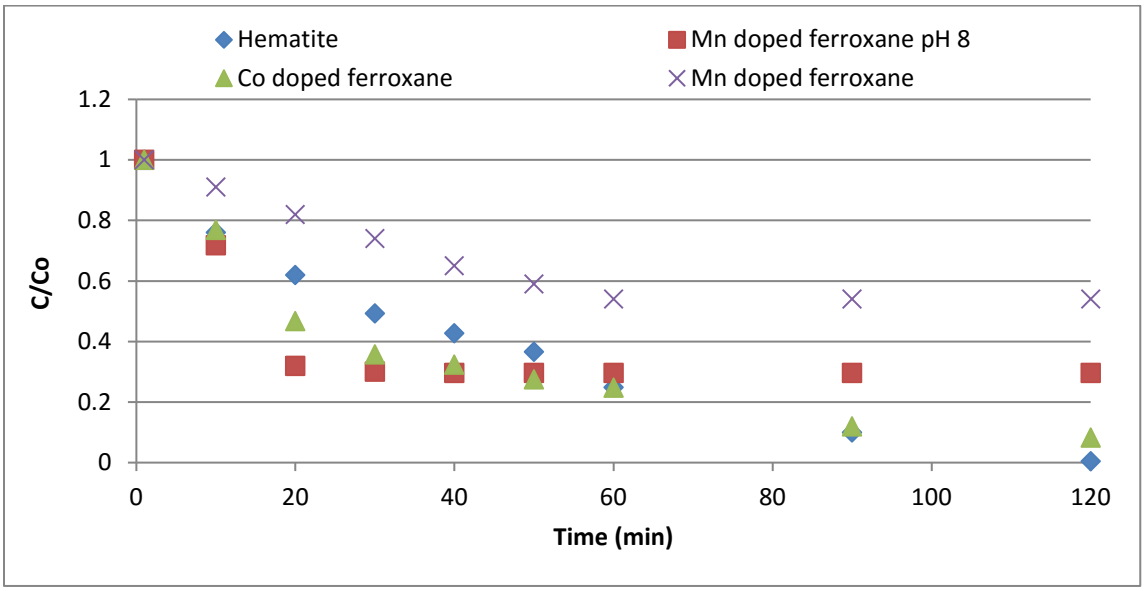

Figure 5.14- Effect Mn, Co doped ferroxane vs Hematite on the degradation of methylene blue under the following conditions: 8 g/l catalyst at Fe: Metal ratio of 2:1, pH 7.6, 10 ppm MB, and UV365. Results from Mn doped ferroxane experiments at pH 8 are added for comparison.

As shown in figure 5.14, experiments with pH 7.6 for Mn doped ferroxane resulted in less degradation than ferroxane alone, about 40% compared to 100 % removal. As the pH was raised to 8 (close the PZC), Mn doped ferroxane nanoparticles achieved 70% degradation within the first 20 minutes, and then no considerable degradation occurred after that. This shows the importance of the PZC: if the pH is far below the pzc, strong electrostatic repulsion between the doped particles and methylene blue causes limited

degradation, which is caused by both the doped particles and methylene blue being positively charged at that pH.

Furthermore, the results show that doped nanoparticles have good potential to catalyze the decomposition rate of H_20_2, since hematite achieved only 40% degradation during the first 20 minutes, while the Mn doped ferroxane achieved 70%. One possible explanation for the limited degradation after 20 minutes is the limitation of available **OH radicals** due to the scavenging effect of H_2O_2 on **OH** radicals (shown in equation 6). The catalyzed decomposition of H_2O_2 by Mn doped ferroxane releases high amounts of **OH** radicals during a short amount of time, which could be beneficial for the degradation of methylene blue. On the other hand, due to the large quantity of H_2O_2 available in the solution, H_2O_2 could also be scavenging the released **OH** radicals, which limits the availability of H_2O_2 in the reaction after 20 minutes to complete the degradation process. Therefore, the system needs to be optimized differently for the metal doped ferroxane experiments by reducing the amount of H_2O_2 added to the solution. This will provide important data that could confirm the hypothesis.

Similar results are noticed for Co doped ferroxane nanoparticles: the nanoparticles achieved faster degradation than hematite during the first 20 minutes, 58% degradation, then the degradation rate slowed down afterwards.

Although the metal doped ferroxane nanoparticles did not achieve 100% degradation like hematite, the results do show the potential of Co and Mn to act as catalysts for Fenton reactions. Further experiments are needed in order to optimize the parameters and achieve 100 % degradation.

5.2.2 Antibiotics degradation

The degradation capability of the optimized Fenton reaction is tested with Sulfamethazine and Oxytetracycline. The results are shown in figures 5.15 and 5.16.

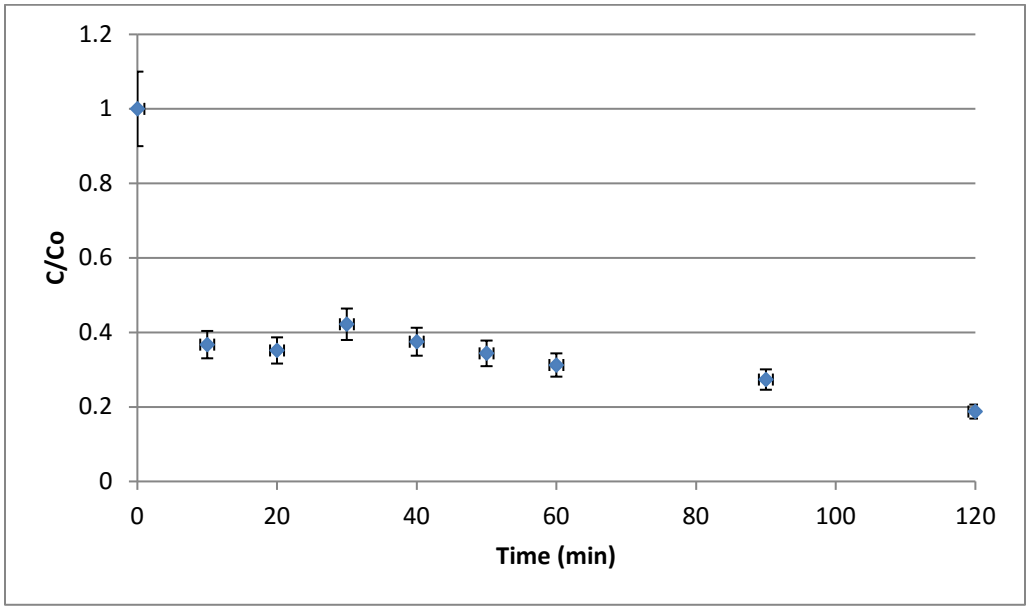

Figure 5.15- Degradation of Sulfamethazine at the following conditions: 1 ppm Sulfamethazine, 8 g/l hematite, 400 mM H_2O_2, UV_{365}, pH= 7.6

As shown in figure 5.15, 80% of Sulfamethazine is removed over a two hour reaction period. The degradation rate is fast during the first 10 minutes of the reaction. That's caused by the fast generation rate of **OH** radicals and the high availability of H_2O_2. After the first 10 minutes, the reaction rate slows down, possibly due to the H_2O_2 being highly consumed during the first 10 minutes, making it a limiting factor in the reaction at later times. Another possible reason for the reaction slowing down could be the scavenging effect of H_2O_2 has on **OH** radicals, as described previously. Therefore, the high availability of H_2O_2 could be a setback in this case. More experimental data is required to prove this theory.

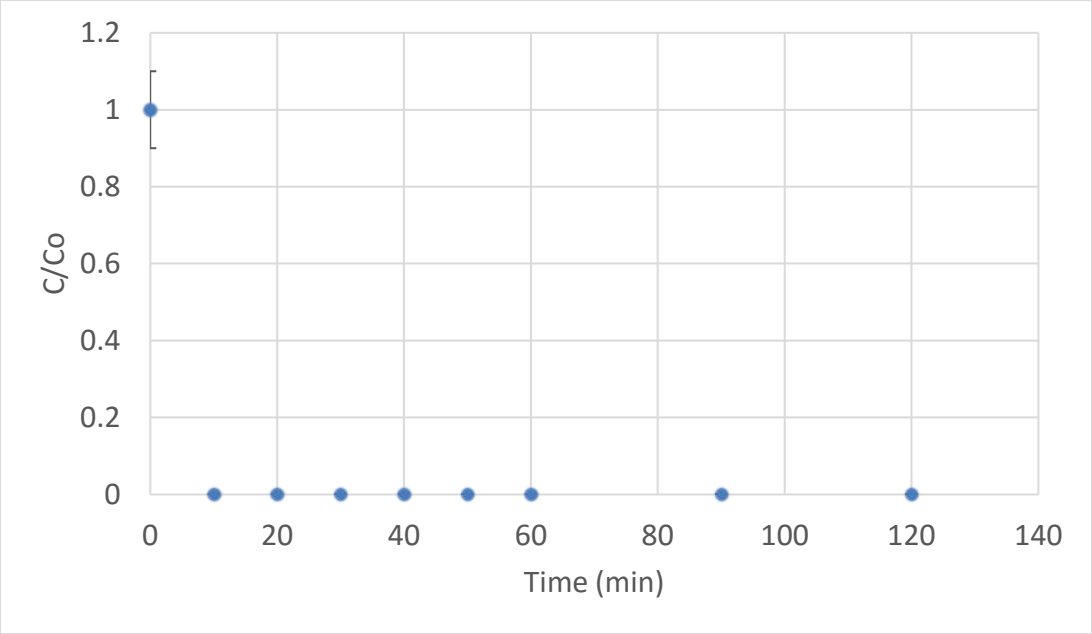

Figure 5.16- adsorption of Oxytetracycline at the following conditions: 1 ppm Oxytetracycline, 8 g/l hematite, pH= 7.6

As shown in figure 5.15, 100% of the Oxytetracycline was adsorbed within 10 minutes of the reactions, hence the addition of H_2O_2 and UV light did not show any further removal. This result is expected, as Oxytetracycline is not as soluble and stable as sulfamethazine, therefore, it's easier to remove. Further experiments are needed with higher concentrations of Oxytetracycline in order to observe the degradation effect of the Fenton reactions.

6 CONCLUSIONS

The concern about pharmaceuticals in water is increasing, and effective, economical treatment methods are needed. Advanced oxidation processes, such as homogenous Fenton processes, have been used in the past; however, the pitfalls of these processes make them expensive and ineffective. In this work, ferroxane nanoparticles are used as catalysts for heterogeneous Fenton reactions in order to overcome the limitations of traditional homogeneous Fenton processes. In addition, ferroxane nanoparticles are doped with Co and Mn in efforts to increase the catalytic activity of the particles.

The work presented in this project shows great potential for ferroxane and the metal doped ferroxane nanoparticles to be used as catalysts for heterogeneous Fenton reactions; which could be used for the degradation of non-biodegradable compounds such as methylene blue and pharmaceuticals in water.

7 FURTHER STUDIES

More experiments are needed in order to optimize the catalytic activity of metal doped ferroxane nanoparticles. The experiments will include the optimization of parameters such as pH, H_2O_2 and catalyst concentrations. The data in this work showed that there's a relationship between the PZC and the degradation rate of the metals. Therefore, the pH of systems should be optimized around the PZC to avoid electrostatic repulsion.

In addition, the catalytic activity of ferroxane-coated ceramic membranes was not tested in this work. Future work will involve degradation experiments using the coated membranes under optimized conditions.

Finally, H_2O_2 decomposition rate, as it reacts with ferroxane and doped ferroxane nanoparticles, needs to be measured using a spectrophotometer. This data will provide valuable information about the catalytic activity of the composites.

REFERENCES

1. Huang, W., *Homogeneous and heterogeneous Fenton and photo-Fenton processes: impact of iron complexing agent ethylenediamine-N, N'-disuccinic acid (EDDS)*. 2012, Université Blaise Pascal-Clermont-Ferrand II.
2. Mazellier, P. and M. Bolte, *Heterogeneous light-induced transformation of 2, 6-dimethylphenol in aqueous suspensions containing goethite.* Journal of Photochemistry and Photobiology A: Chemistry, 2000. **132**(1): p. 129-135.
3. Leland, J.K. and A.J. Bard, *Photochemistry of colloidal semiconducting iron oxide polymorphs.* Journal of Physical Chemistry, 1987. **91**(19): p. 5076-5083.
4. Cornell, R.M. and U. Schwertmann, *The iron oxides: structure, properties, reactions, occurrences and uses*. 2003: John Wiley & Sons.
5. Schwertmann, U. and R. Cornell, *Iron oxides in the laboratory. VCH Publ*. 1991, Weinheim, Germany.
6. Rahman, M.A., S.R. Amin, and A.S. Alam, *Removal of methylene blue from waste water using activated carbon prepared from rice husk.* Dhaka University Journal of Science, 2012. **60**(2): p. 185-189.
7. Forgacs, E., T. Cserhati, and G. Oros, *Removal of synthetic dyes from wastewaters: a review.* Environment international, 2004. **30**(7): p. 953-971.
8. Program, N.T., *Executive summary of safety and toxicity information for methylene blue trihydrate 7220-79-3.* US Department of Health and Human Services, 1990.
9. Gustafson, R.H. and R.E. Bowen, *Antibiotic use in animal agriculture.* Journal of Applied Microbiology, 1997. **83**(5): p. 531-541.
10. McEwen, S.A. and P.J. Fedorka-Cray, *Antimicrobial Use and Resistance in Animals.* Clinical Infectious Diseases, 2002. **34**(Supplement 3): p. S93-S106.
11. Visek, W., *The mode of growth promotion by antibiotics.* Journal of Animal Science, 1978. **46**(5): p. 1447-1469.
12. Hamscher, G., et al., *Determination of persistent tetracycline residues in soil fertilized with liquid manure by high-performance liquid chromatography with electrospray ionization tandem mass spectrometry.* Analytical Chemistry, 2002. **74**(7): p. 1509-1518.
13. Kumar, K., et al., *Antibiotic uptake by plants from soil fertilized with animal manure.* Journal of Environmental Quality, 2005. **34**(6): p. 2082-2085.
14. Kang, D.H., et al., *Antibiotic Uptake by Vegetable Crops from Manure-Applied Soils.* Journal of Agricultural and Food Chemistry, 2013. **61**(42): p. 9992-10001.
15. Thiele-Bruhn, S., *Pharmaceutical antibiotic compounds in soils–a review.* Journal of Plant Nutrition and Soil Science, 2003. **166**(2): p. 145-167.
16. Hirsch, R., et al., *Occurrence of antibiotics in the aquatic environment.* Science of the Total Environment, 1999. **225**(1): p. 109-118.
17. Cabello, F.C., *Heavy use of prophylactic antibiotics in aquaculture: a growing problem for human and animal health and for the environment.* Environmental microbiology, 2006. **8**(7): p. 1137-1144.
18. Levy, S.B., *Antibiotic resistance: an ecological imbalance.* Antibiotic resistance: origins, evolution, selection and spread, 1997. **207**: p. 1-14.
19. Khachatourians, G.G., *Agricultural use of antibiotics and the evolution and transfer of antibiotic-resistant bacteria.* Canadian Medical Association Journal, 1998. **159**(9): p. 1129-1136.

20. Droste, J.H.J., et al., *Does the use of antibiotics in early childhood increase the risk of asthma and allergic disease?* Clinical & Experimental Allergy, 2000. **30**(11): p. 1548-1553.
21. Batt, A.L., S. Kim, and D.S. Aga, *Comparison of the occurrence of antibiotics in four full-scale wastewater treatment plants with varying designs and operations.* Chemosphere, 2007. **68**(3): p. 428-35.
22. Ben, W., et al., *Removal of veterinary antibiotics from sequencing batch reactor (SBR) pretreated swine wastewater by Fenton's reagent.* Water Res, 2009. **43**(17): p. 4392-402.
23. Uslu, M.Ö. and I.A. Balcıoğlu, *Comparison of the ozonation and Fenton process performances for the treatment of antibiotic containing manure.* Science of the total environment, 2009. **407**(11): p. 3450-3458.
24. Yang, T., et al., *Development of a sensitive monoclonal antibody-based ELISA for the detection of sulfamethazine in cow milk, honey, and swine urine.* Hybridoma, 2010. **29**(5): p. 403-407.
25. ElSayed, E.M., S.O. Prasher, and R.M. Patel, *Effect of nonionic surfactant Brij 35 on the fate and transport of oxytetracycline antibiotic in soil.* Journal of environmental management, 2013. **116**: p. 125-134.
26. Hofs, B., et al., *Comparison of ceramic and polymeric membrane permeability and fouling using surface water.* Separation and Purification Technology, 2011. **79**(3): p. 365-374.
27. Mueller, U., G. Biwer, and G. Baldauf, *Ceramic membranes for water treatment.* Water Science and Technology: Water Supply, 2010. **10**(6): p. 987-994.
28. Mueller, U. and M. Witte, *Ceramic membranes-Case related protocol for optimal operational conditions to treat filter backwash water.* Deliverable number D, 2007. **2**(3.5).
29. Cortalezzi, M.a.M., et al., *Ceramic membranes derived from ferroxane nanoparticles: a new route for the fabrication of iron oxide ultrafiltration membranes.* Journal of membrane science, 2003. **227**(1): p. 207-217.
30. Rose, J., et al., *Synthesis and characterization of carboxylate-FeOOH nanoparticles (ferroxanes) and ferroxane-derived ceramics.* Chemistry of Materials, 2002. **14**(2): p. 621-628.
31. Sabbatini, P., et al., *Fabrication and characterization of iron oxide ceramic membranes for arsenic removal.* Water research, 2010. **44**(19): p. 5702-5712.
32. Sawyer;, C.N., P.L. McCary;, and G.F. Perkin, *Chemistry for Environmental Engineering*. 1994, New York: McGraw-Hill.
33. Fidalgo de Cortalezzi, M.M., et al., *Virus removal by iron oxide ceramic membranes.* Journal of Environmental Chemical Engineering, 2014. **2**(3): p. 1831-1840.
34. Cruz, N.D.l., et al., *Degradation of emergent contaminants by UV, UV/H2O2 and neutral photo-Fenton at pilot scale in a domestic wastewater treatment plant.* Water Research, 2013. **47**: p. 5836-5845.
35. Wang, Q., S. Tian, and P. Ning, *Degradation mechanism of methylene blue in a heterogeneous Fenton-like reaction catalyzed by ferrocene.* Industrial & Engineering Chemistry Research, 2013. **53**(2): p. 643-649.
36. Kiwi, J., C. Pulgarin, and P. Peringer, *Effect of Fenton and photo-Fenton ractions on the degradation and biodegradability of 2 and 4-nitrophenols in water treatment.* Applied Catalysis B: Environmental, 1994. **3**: p. 335-350.

37. Lee, Y., et al., *Influence of various reaction parameters on 2,4-D removal in photo/ferrioxalate/H2O2 process.* Chemosphere, 2003. **51**: p. 901-912.
38. Sabhi, S. and J. Kiwi, *Degradation Of 2,4-Dichlorophenol By Immobilized Iron Catalysts.* Water Research, 2001. **35**(8): p. 1994-2002.
39. Xu, L. and J. Wang, *Fenton-like degradation of 2,4-dichlorophenol using Fe 3O 4 magnetic nanoparticles.* Applied Catalysis B: Environmental, 2012. **123-124**: p. 117-126.
40. Mitsika, E., C. Christophoridis, and K. Fytianos, *Fenton and Fenton-like oxidation of pesticide acetamiprid in water samples: Kinetic study of the degradation and optimization using response surface methodology.* Chemosphere, 2013. **93**: p. 1818-1825.
41. Li, R., et al., *Removal of triazophos pesticide from wastewater with Fenton reagent.* Journal of Hazardous Materials, 2009. **167**: p. 1028-1032.
42. Luca, A.D., et al., *Atrazine Removal in Municipal Secondary Effluents by Fenton and Photo-Fenton*

Treatments. Chemical Engineering and Technology, 2013. **36**(12): p. 2155-2162.
43. Micó, M.M., et al., *Fosetyl-Al photo-Fenton degradation and its endogenous catalyst inhibition.* Journal of Hazardous Materials, 2014. **265**: p. 177-184.
44. Chen, F., et al., *Photo-Fenton degradation of dye in methanolic solution under both UV and visible irradiation.* Journal of Photochemistry and Photobiology A: Chemistry, 2001. **138**(2): p. 139-146.
45. Du, W., Y. Xu, and Y. Wang, *Photoinduced Degradation of Orange II on Different Iron (Hydr)oxides in Aqueous Suspension: Rate Enhancement on Addition of Hydrogen Peroxide, Silver Nitrate, and Sodium Fluoride.* Langmuir, 2008. **24**(1): p. 175-181.
46. Valentine, R.L. and H.C.A. Wang, *Iron Oxide Catalyzed Oxidation of Quinoline By Hydrogen Peroxide.* Journal of Environmental Engineering, 1998. **124**(1): p. 31-38.
47. Pignatello, J.J., E. Oliveros, and A. MacKay, *Advanced Oxidation Processes for Organic Contaminant Destruction Based on the Fenton Reaction and Related Chemistry.* Critical Reviews in Environmental Science and Technology, 2006. **36**(1): p. 1-84.
48. Benjamin, M.M. and D.F. Lawler, *Water Quality Engineering: Physical / Chemical Treatment Processes*. 2013: Wiley.
49. Neyens, E. and J. Baeyens, *A review of classic Fenton's peroxidation as an advanced oxidation technique.* Journal of Hazardous Materials, 2003. **B98**: p. 33-50.
50. Araujo, F., et al., *Heterogeneous Fenton process using the mineral hematite for the discolouration of a reactive dye solution.* Brazilian Journal of Chemical Engineering, 2011. **28**(4): p. 605-616.
51. David, F. and P.G. David, *Photoredox chemistry of iron(III) chloride and iron(III) perchlorate in aqueous media. A comparative study.* The Journal of Physical Chemistry, 1976. **80**(6): p. 579-583.
52. Pinto, I.S.X., et al., *Nanostructured delta-FeOOH: An efficient Fenton-like catalyst for the oxidation of organics in water.* Applied Catalysis B: Environmental, 2012. **119-120**: p. 175-182.
53. Ai, Z., et al., *Fe@Fe2O3 Core-shell nanowires as iron reagent. 1. Efficient degradation of rhodamine by a novel sono-fenton process.* Journal of Physical Chemistry C, 2007. **111**(11): p. 4087-4093.
54. Costa, R.C.C., et al., *Novel active heterogeneous Fenton system based on Fe3−xMxO4 (Fe, Co, Mn, Ni): The role of M2+ species on the reactivity towards H2O2 reactions.* Journal of Hazardous Materials, 2006. **B128**: p. 171-178.

55. Santos, L., A. Meireles, and L. Lange, *Degradation of antibiotics norfloxacin by Fenton, UV and UV/H2O2.* Journal of environmental management, 2015. **154**: p. 8-12.
56. Schwertmann;, U. and R.M. Cornell, *Iron Oxides in the Laboratory. Preparation and Characterisation*. 1991, New York: VCH.
57. Callender, R.L. and A. Barron, *Facile Synthesis of Aluminum-containing Mixed-Metal Oxides Using Doped Carboxylate Alumoxane Nanoparticles.* Journal of the American Ceramic Society, 2000. **83**(7): p. 1777-1789.
58. Cortalezzi, M.M.F.d., et al. *Synthesis and characterization of Manganese doped ferroxane nanoparticles*. in *Material Research Society Symposium AA, 2003 Fall Meeting*. 2003. Boston, MA.
59. Hayes, P., *Process Principles in Minerals and Materials Production, 3rd Edition*. 2003: Hayes Publishing Co.
60. Cullity, B.D., *Elements of X-Ray Diffraction, 2nd Edition*. 1978, Reading, Massachusetts: Addison-Wesley Publishing Company.
61. Berg, J., *An Introduction to Interfaces & Colloids: The Bridge to Nanoscience*. 2010, Hackensack, NJ: World Scientific Publishing Co.
62. Brunauer, S., P.H. Emmett, and E. Teller, *Adsorption of Gases in Multimolecular Layers.* Journal of the American Chemical Society, 1938. **60**(2): p. 309-319.
63. Bindell, J., *Scanning Electron Microscopy*. Encyclopedia of Materials Characterization: Surfaces, Interfaces, Thin Films, ed. R. Brundle and C. Evans. 1992, Greenwich: Manning Publication Company.
64. De Angelis, L. and M.M. Fidalgo de Cortalezzi, *Ceramic membrane filtration of organic compounds: Effect of concentration, pH, and mixtures interactions on fouling.* Separation and Purification Technology, 2013. **118**: p. 762.